





Research article

Synthesis and characterization of biodegradable–electroactive polymer–Au nanocomposite materials for H₂S sensing

Aamna Bibi¹, Ying-Hsuan Li¹, Hsi-Wei Jia¹, Hsien-po Kuo¹, Nadaraj Sathishkumar¹, Hsin-Tsung Chen¹, Karen S. Santiago², Jui-Ming Yeh^{1*}

¹Department of Chemistry, Center for Nanotechnology and R & D Center for Membrane Technology at Chung Yuan Christian University, 32023 Chung Li, Republic of China

²Department of Chemistry, College of Science; Research Center for the Natural and Applied Sciences, University of Santo Tomas, España, 1015 Manila, Philippines

Received 24 February 2022; accepted in revised form 11 June 2022

Abstract. In this paper, a series of biodegradable–electroactive polymers (BEP) and its composite with gold nanoparticles (BEP–Au) were prepared and used in the detection of H₂S gas. First, the starting materials which included the electroactive aniline tetramer (ACAT) and biodegradable polylactic acid (PLA) were synthesized and characterized. The BEP was then prepared by reacting tri-isocyanate (N-3300) with the synthesized ACAT and PLA at a specific feeding ratio. In this case, ACAT served as a pendant group. The BEP–Au composite was subsequently prepared by immersing a specific amount of BEP in a certain concentration of HAuCl₄·3H₂O solution for 6 h, followed by characterization. The gas sensing performances of as-prepared sensors were tested. Results revealed that the BEP sensor has a good sensitivity of 0.0114 ppm⁻¹ towards increasing concentrations of H₂S gas (1–20 ppm), which was observed to have increased up to 0.907 ppm⁻¹ after the addition of gold nanoparticles, *i.e.*, BEP–Au. Furthermore, the said sensors also showed rapid response and recovery rates, good repeatability, and high selectivity. To fully evaluate the feasibility of BEP and BEP–Au for the detection of H₂S gas, the adsorption was further investigated via the *ab initio* density functional theory (DFT). The DFT calculations complemented the experimental gas sensing results.

Keywords: biodegradable polymers, composite, Au nanoparticles, H₂S gas sensing

1. Introduction

Among the array of conducting polymers, polyaniline (PANI) has received the most attention owing to its unique properties resulting in numerous applications [1, 2]. For example, PANI has a reversible redox activity with a relative electrode potential greater than that of active metals, alloys, and chromate couple, indicating that it can be applied as a corrosion inhibitor [3] supercapacitor in batteries and fuel cells [4]. Also, PANI has been investigated for its potential gas sensor applications because it can be easily doped/dedoped under an acidic or

alkaline environment [5]. For instance, Gautam *et al.* [6] studied the effects of moisture in the environment and molecular weight of PANI on H₂S sensing characteristics. Reddy *et al.* [7] developed a porous CaMnO₃ doped polyaniline nanocomposite thin films by doping CaMnO₃ by weight percentage (5, 10, 15, 20, and 25%) in an aqueous solution of polyaniline using chemical polymerization technique. The H₂S gas was used to study the gas sensing behavior of investigated films. In 2021, Zuo *et al.* [8] fabricated an amperometric H₂S gas sensor using ultrathin Pt NTs.

*Corresponding author, e-mail: juiming@cycu.edu.tw

© BME-PT

However, the main problem with PANI is its poor solubility which limits its applications [9]. Therefore, the synthesis and applications of aniline oligomer-based polymers, such as polyimide, epoxy resin, and polyurethane, have attracted intensive research interest in the past decade [10]. Electroactive polymers (EAPs) [11, 12] are derived from aniline oligomers and utilized in various applications [13–20]. EAPs have also been used in sensing applications. Tsai *et al.* [18] developed an aniline-pentamer/Au-based electrochemical sensor for sensing ascorbic acid. Similarly, Bibi *et al.* [19] devised electroactive composites by using aniline-tetramer/nanoparticles (Ag, Pt, and Au) for sensing uric acid. Zaho *et al.* [21] constructed a floating-gate ion-sensitive field-effect transistor by using an aniline-trimer for sensing ammonia gas (70 ppm). Bibi *et al.* [10] formulated an electroactive polyamic acid that contains an aniline trimer in the main chain for sensing H₂S gas. Over the past two decades, interest in the application of biodegradable polymers in both academic and industrial fields has intensified [22]. The use of biodegradable polymers is being promoted to ensure sustainable development because of environmental pollution and waste management issues. Biodegradable polymers may have positive environmental and economic effects as they reduce the need for synthetic polymers at low costs [23]. Among biodegradable polymers, aliphatic polyesters with a hydrolyzable backbone are the most extensively studied class because of their diversity and synthetic versatility [24]. Polylactide (PLA), an aliphatic polyester, is regarded as the most environmentally friendly polymeric substitute because of its biodegradability, biocompatibility, and good thermomechanical properties. Initially, its applications were limited to biomedicine and packaging, but now PLA is viewed as a valuable biosourced polymer in electronics and automotive [25–31]. Marasso *et al.* [32] fabricated a 3D-printed smart cap embedded with a resistive temperature sensor made of a conductive PLA filament. Luo *et al.* [33] developed a wireless radio frequency microelectromechanical system (RF MEMS) pressure sensor, zinc/iron bilayers were used as the sensor conductor material, and known biodegradable polymers poly-L-lactide and polycaprolactone were used as dielectric and structural materials. Mallick *et al.* [34] constructed a humidity sensor and assessed the capacitive and

resistive response of PLA/TiO₂ nanocomposite films under relative humidity levels ranging from 20 to 90%. Katseli *et al.* [35] used a carbon-loaded PLA conductive filament for electrochemical sensing of caffeine, mercury, and glucose. Silva *et al.* [36] utilized a 3D-printed reduced graphene oxide/polylactic acid electrode for biosensing of serotonin and catechol. In 2020, Zhang *et al.* [37] designed a biosensor by utilizing PLA-OPPy-Au NPs-Nafion composite for glucose detection. Sathies *et al.* [38] devised an FDM-printed conductive PLA-carbon black sensor for sensing volatile organic compounds (VOCs). Kumar *et al.* [39] created a PLA/CNT-based transducer for detecting VOCs and assessing air quality.

Thus, biodegradable-electroactive polymers (BEPs) are of great interest for various applications, particularly in biomedicine [40–45]. BEPs are also used in sensing applications. Gautam *et al.* [46] reported a ternary green nanocomposite based on PANI/multiwalled carbon nanotube (MWCNT)/carboxymethyl cellulose (CMC) for electrochemical sensing of ascorbic acid. Macagnano *et al.* [47] developed an environmentally friendly conductive chemosensor on the basis of the biodegradable-conductive polymer blend of polyaniline/poly-3-hydroxybutyrate for measuring gases and VOCs in moist environments.

In the present work, we developed for the first time an environment-friendly conductive sensor for monitoring H₂S gas using composites of BEP and gold nanoparticles (Au-NPs). The Au-NPs is an effective means to improve the sensing performance of polymer-based gas sensors via catalytic effect [48–50]. To the best of our knowledge, BEP-Au composites have never been tested in sensing applications thus far. BEP was synthesized via copolymerization of biodegradable PLA and amino-capped aniline-tetramer (ACAT) as the electroactive part. BEP had the hydrolyzable backbone of PLA, which bore ACAT as the pendant group. The gas-sensing performance of the BEP-Au sensors was measured at room temperature in 60% relative humidity (RH). The performance of the BEP and BEP-Au sensors in adsorbing H₂S gas was evaluated via the *ab initio* density-functional theory (DFT). The stable adsorption structure of the H₂S molecule on the BEP and BEP-Au sensors was demonstrated. Adsorption energies and charge transfer were calculated to evaluate the adsorption abilities of the BEP and Au-doped BEP sensors to H₂S gas.

2. Experimental section

2.1. Chemicals and instrumentation

Hydrazine (N_2H_4) and *N*-phenyl-*p*-phenylenediamine (Alfa Aesar, Shore road, Heysham, England), ammonium persulfate (APS, 97.0%, J. T. Baker, Avantor Performance Materials, LLC, Randor, Philadelphia), 1,4-butanediol (BDO), dichloromethane (DCM), tetrahydrofuran (THF) and 3,6-dimethyl-1,4-dioxane-2,5-dione (NMP) (Macron Fine Chemicals, Avantor Performance Materials, LLC, Randor, Philadelphia), tin (II) 2-ethylhexanoate (MP Bio-medicals, Inc. IIIkirch, France), Desmodur[®]N3300A (Covestro, Taoyuan, Taiwan), ethanol (C_2H_5OH , ECHO Chemical Co., LTD, Toufen city, Miaoli, Taiwan), dimethylformamide (DMF, 99.8%, Honeywell Riedel-de Haen, Seetze, Germany), ammonium hydroxide (NH_4OH , 25%, Honeywell Fluka, Wunsrofer strasse 40, Seetze, Germany), $HuCl_4 \cdot 3H_2O$ (Thermo Fischer Scientific, 30 Bond street, Ward Hill, USA) were all used as received without further treatment. All the gases, including H_2S (50 ppm + N_2), SO_2 (50 ppm + N_2), NH_3 (50 ppm + N_2), NO_2 (50 ppm + N_2), CO (50 ppm + N_2), CO_2 , N_2 , and air (Chian Hong Gas Co., LTD) used in this study were used as received. In carrying out gas sensing studies, indium-tin-oxide (ITO) inter-digitated electrode was used to prepare the sensors (12 pairs of electrodes, 0.3 mm spacing, and $l \times w$ of 20×20 mm).

Proton nuclear magnetic resonance (1H -NMR) spectra were performed on a Bruker 300 spectrometer (USA). Fourier-transform infrared spectroscopy (FTIR) spectra were recorded at a resolution of 4.0 cm^{-1} using an FTIR spectrometer (JASCO, FT/IR-4200, Japan). Mass spectra were measured on a Bruker Daltonics IT mass spectrometer model Esquire 2000 (Leipzig, Germany) equipped with an Agilent ESI source (model G1607-6001). Degradability test was performed in DENG YNG water bath G-10 (Dogger, Taipei, Taiwan). Weight-average and number-average molecular weights of EBPU were tested on a Waters GPC-150CV (Waters International Corporation Taipei, Taiwan) equipped with a differential refractometer detector and a Styragel HT column using NMP as eluent and monodisperse polystyrene as calibration standards. UV-visible absorption spectroscopy was carried out using a JASCO V-750 (Sunway Scientific corporation, Japan). Cyclic voltammetry (CV) was conducted on an AutoLab PGSTAT 204 (Ω Metrohm Autolab, KM Utrecht, The Netherlands) electrochemical workstation. The

morphology and nature of the composite was confirmed by using scanning electron microscopy (SEM, JEOL JSM-7600F, Japan) and X-ray powder diffraction XRD (Bruker, D8 advance, Panalytical, X'Pert Pro).

2.2. Synthesis of amino-capped aniline-tetramer (ACAT)

ACAT was synthesized as follows. First, 3.68 g (20 mmol) of *N*-phenyl-*p*-phenylenediamine was dissolved in 400 ml of nitric acid aqueous solution (352 ml H_2O , 48 ml HNO_3 , 600 ml DMF) under stirring at $0^\circ C$ (labeled as beaker A). Subsequently, 2.50 g (10 mmol) of ammonium persulfate was dissolved in a 20 ml nitric acid aqueous solution maintained at $0^\circ C$ (labeled as beaker B). Afterward, the solution of beaker B was introduced dropwise into beaker A and then reacted for 3 h. The as-obtained acid-doped precipitation was collected by suction. Finally, the acid-doped precipitation was dispersed into 400 ml of 1.0 N NH_4OH aqueous solution under stirring for 24 h, followed by suction and dynamic drying at $40^\circ C$ for 24 h to obtain a fine blue powder with a yield of $\sim 35\text{ wt}\%$ [51].

2.3. Synthesis of poly(lactic acid) (PLA)

The lactide or 3,6-dimethyl-1,4-dioxane-2,5-dione was freeze-dried for 24 h prior to use. The dried lactide (7.2 g 0.05 moles) was poured into a three-necked bottle and subjected to reflux at $140^\circ C$ under nitrogen gas. Two drops of $Sn(oct)_2$ were then added to the flask after complete melting, and the reaction was run for 6.5 h. Afterward, 0.343 g (3.8 mmol) of BDO was added, and the chemical reaction was run for another 1.5 h. Subsequently, the reaction mixture was allowed to cool down to room temperature. DCM (20 ml) was added, and then ethanol (400 ml) was added dropwise to precipitate PLA. The PLA precipitates were filtered and washed with DCM (10 ml) and ethanol (200 ml). At the final step, PLA was dried in a vacuum oven at $55^\circ C$ for 2 h.

2.4. Preparation of the biodegradable-electroactive polymer (BEP)

BEP was prepared following Figure 1. First, 0.948 g (1.88 mmol) of Desmodur[®] N3300A was introduced into a three-necked round-bottom flask containing 6 ml of THF/DMF co-solvent ($v/v = 1:1$) and stirred for 30 min. Nitrogen gas was bubbled into the flask throughout the reaction. Afterward, 0.348 g of ACAT

(0.466 mole) dissolved in 6 ml of THF/DMF ($v/v = 1:1$) was added dropwise to the previous flask and stirred further for 3 h. Subsequently, 3 g (0.466 mmol) of the as-prepared PLA and 0.042 g (0.466 mmol) of 1,4-butanediol dissolved in 8 ml of THF/DMF co-solvent ($v/v = 1:1$) was added and stirred for another 3 h. Finally, the blue BEP solid was obtained upon drying under a dynamic vacuum at 55 °C for 2 h with a good yield of ~50 wt%.

2.5. Preparation of BEP-Au composite materials

BEP–Au composites were also prepared via Figure 1. First, 0.1 g of BEP was dispersed into 10 ml of 1.0 N NH_4OH aqueous solution containing 1 ml of N_2H_4 and then stirred for 24 h. Afterward, the BEP sus-

pension was filtered and then washed with an excess amount of distilled water until the pH value of the resultant washing water reached 7. The as-obtained reduced BEP was then freeze-dried for 24 h. Subsequently, 0.1 g of the reduced form of BEP fine powder was introduced into 19 ml of $\text{HAuCl}_4 \cdot 3\text{H}_2\text{O}$ aqueous solution (10 mmol) [52] for 6 h. Finally, the solution was centrifuged and filtered to collect the BEP–Au composite material. (The real weight ratio between BEP and Au determined via TGA was 96.5% and 3.5%, respectively).

2.6. Conductivity

The electrical conductivity (σ , [S/cm]) of BEP and BEP–Au was measured using a four-point probe. The thin films were produced on an ITO by drop-coating

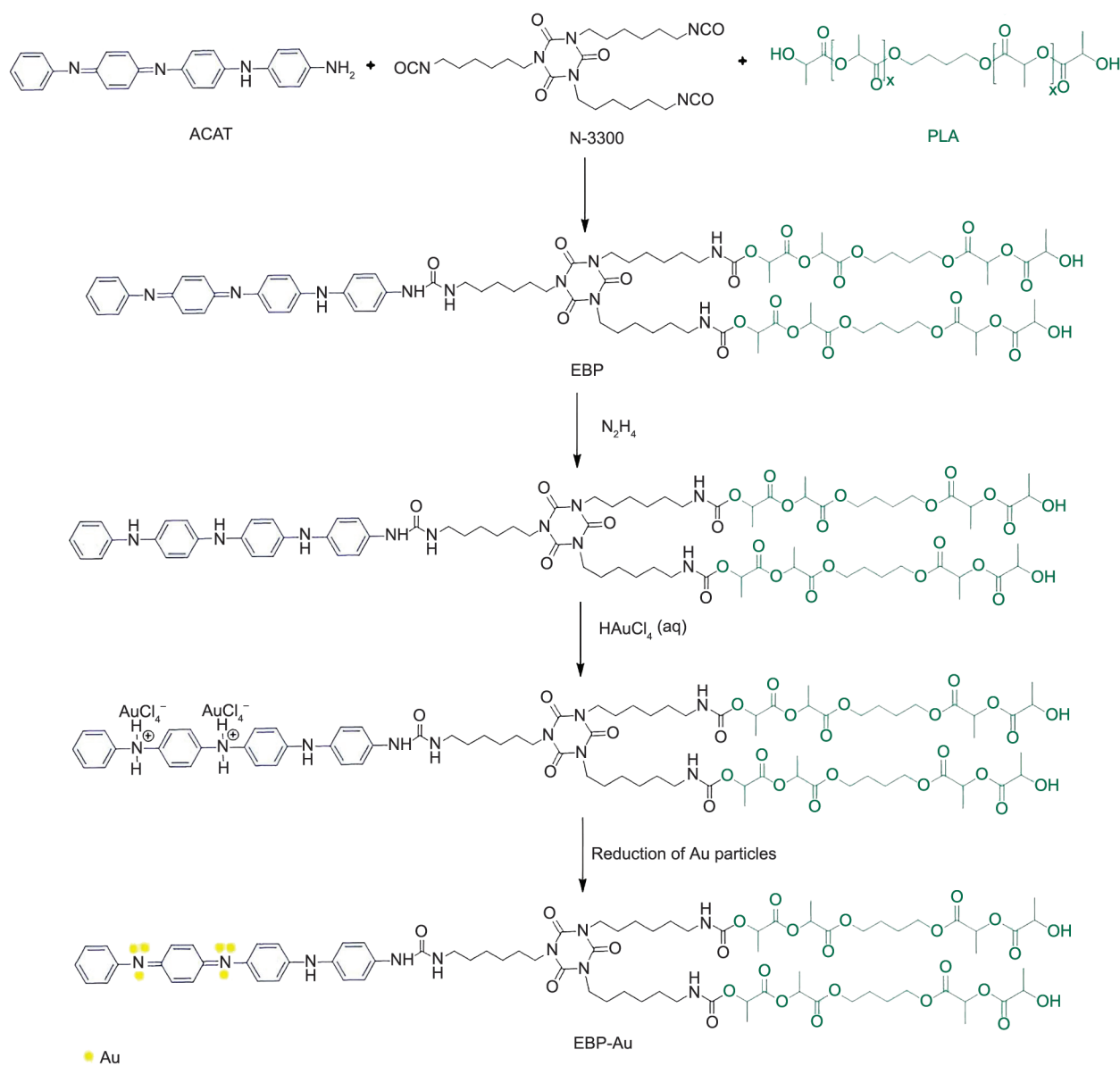


Figure 1. Flowchart for the preparation of BEP-Au composite material.

and then dried in a vacuum for 2 h. After that, as prepared films were doped by using H₂S gas (20 ppm) for about 10 min. These ITO were then placed on the four-probe apparatus, and the corresponding electrical current was obtained after providing voltage. Three measurements were taken for each sample [53].

2.7. Cyclic voltammetry (CV)

The redox behavior of EBP and the composites were examined via electrochemical cyclic voltammetry (CV) in 1 M H₂SO₄ with a scan rate and a scan range of 100 mV/s and 0.0–1.0 V, respectively, on the Auto-Lab PGSTAT 204 electrochemical workstation. The working electrode was prepared by spin-coating the EBP and BEP–Au solutions in THF:DMF (1:1) solvent on an ITO and then dried in a vacuum oven for 1 h. A platinum wire and a saturated calomel electrode were used as a counter and a reference electrode, respectively. All CV measurements were repeated thrice.

2.8. Biodegradability of BEP and BEP–Au composite

The hydrolytic degradation of the synthesized films was monitored by placing dried films in a tube filled with PBS (pH 7.4). The tube was then placed in a water bath (DENG YNG G-10) at 37 °C. The samples were removed at different intervals, washed with deionized water, completely dried in a vacuum, and weighed to determine any reduction. Weight loss percentage was calculated as Equation (1):

$$\text{Weight loss [\%]} = \frac{W_1 - W_2}{W_1} \cdot 100 \quad (1)$$

where W_1 and W_2 represent the weights of the films before and after degradation, respectively. An average value of three different samples was recorded [54].

2.9. Fabrication of ITO inter-digitated electrode (IDE) coated with BEP and BEP–Au composites

The ITO coated with the as-prepared samples was constructed via the spin-coating technique. The EBP and EBP–Au solutions (1 wt%) were prepared by dissolving 0.1 g of the respective sample in 10 g of THF/DMF (1:1) while stirring at room temperature. Afterward, thin films were prepared by spin-coating a 500 μ l solution on an ITO at 2000 rpm. The BEP- and BPE–Au-coated ITO sensors were then dried in a vacuum oven for 2 h prior to use in gas sensing.

2.10 H₂S sensing studies of ITO coated with BEP and BEP–Au composites

The gas-sensing performance of the sensors was assessed using air as carrier gas (1000 sccm) at 25 \pm 0.5 °C and relative humidity (RH) of 60%. Stable current values (I/I_0) in the air were obtained before the target gas was introduced. A certain amount of H₂S gas was introduced into the gas chamber for an interval of 120 s, and the response was recorded in terms of a normalized current on a Keithlink probing and measurement system (Keithlink Technology Co. Ltd). A fixed voltage of 1 V was applied, and the resulting change in the electrical conductivity of the BEP and composites was reported as the corresponding gas response [47, 55–59] (Equation (2)):

$$\text{Response} = \frac{I}{I_0} \quad (2)$$

where I_0 and I represent the conductance of the material in air and upon exposure to H₂S gas, respectively.

2.11. Computational method

All calculations were performed using the Gaussian09 suite programs. Geometry optimizations were calculated in the gas phase via *ab initio* DFT calculations with a B3LYP hybrid functional [60]. In all calculations, the LANL2DZ basis set [61] was chosen for the Au atom and the 6–31+g(*d*, *p*) basis set for C, H, N, O, and S atom-containing molecules. Mulliken charge analysis was performed to determine the charge distribution of the systems. Adsorption energies (E_{ads}) were calculated using the following equation to evaluate the interaction of H₂S molecules with the adsorbents (Equation (3)):

$$E_{\text{ads}} = E_{\text{sur/H}_2\text{S}} - (E_{\text{H}_2\text{S}} + E_{\text{sur}}) \quad (3)$$

where E_{sur} , $E_{\text{H}_2\text{S}}$ and $E_{\text{sur/H}_2\text{S}}$ are the total energy of the surface, adsorbate (H₂S), and adsorbate on the surface, respectively. A more negative value denotes a stronger interaction between the adsorbate and the surface. The recovery time of H₂S was predicted from Equation (4) [62]:

$$\tau = \vartheta_0 - \exp(-E_{\text{ads}}/kT) \quad (4)$$

where k is the Boltzmann's constant ($8.62 \cdot 10^{-5}$ eV/K), T is the temperature (298 K), and ϑ_0 refers to the attempt frequency ($\vartheta_0 = 10^{12}$ s⁻¹).

3. Results and discussion

3.1. Characterisation

FTIR analysis demonstrated that the BEP and BEP–Au sensors were successfully synthesized. The FTIR spectra of ACAT, N-3300, PLA, BEP, and BEP–Au composites are shown in Figure 2. In the curves of BEP, an absorption peak was observed at 1660 cm^{-1} , which can be ascribed to the successful formation of the amide group between the hydroxyl groups of PLA and the isocyanate group of N-3300. The absence of the characteristic absorption at 2276 cm^{-1} indicated that the $-\text{NCO}$ group was completely consumed. The absorption peak at 3387 cm^{-1} suggested the formation of a urea group. On the other hand, the absorption of benzenoid and quinoid rings stretching at 1503 and 1459 cm^{-1} appeared in the BEP curve, proving the existence of the ACAT segment as the pendant group [63]. The molecular weight of the as-prepared BEP was determined via GPC analysis ($M_w = 4652\text{ g/mol}$, $M_n = 3086\text{ g/mol}$, and $PDI = 1.5$). The curves of the BEP and BEP–Au composites contained the characteristic peaks of all segments, indicating that they were successfully prepared.

For the BEP–Au films, the absorbance of almost all bands slightly decreased, and its broadness increased relative to BEP. The BEP–Au composites showed almost the same absorption peaks as BEP, indicating that no new bond was formed or no strong chemical interaction occurred within the composites [64, 65]. Energy-dispersive X-ray spectroscopy (EDX) analysis of the BEP–Au composites revealed the presence of Au-NPs. A representative scanning electron microscope image of BEP–Au composite is shown in

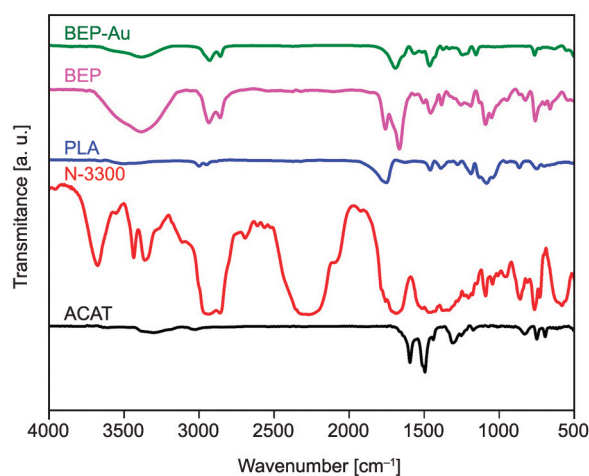


Figure 2. FTIR spectra of ACAT, N-3300, PLA, BEP, and BEP–Au composite.

Figure 3a. The EDX spectra of the BEP–Au composites are given in Figure 3b. An optical absorption band peak appeared at approximately 2.2 keV , which is the typical absorption of metallic gold nanoparticles. Elemental mapping analysis of Au-NPs showed an extreme distribution of metallic gold in the scanned electron micrograph image of the Au-NP pellet solution (Figure 3c).

The XRD patterns of the BEP and BEP–Au composites are provided in Figure 3d. The XRD pattern of BEP showed a broad peak, which is a characteristic diffraction behavior of an amorphous polymer. The XRD patterns of the BEP–Au composites unveiled four diffraction peaks at 2θ of 38.62 , 44.72 , 65.02 , and 77.84° , which could be attributed to the (111), (200), (220), and (311) planes, respectively, of face-centered cubic-shaped crystalline Au-NPs [66]. Furthermore, the TEM morphological characteristics of the Au-NPs showed that the NPs obtained had a clear morphology (Figure 3e). The Au-NPs synthesized herein were spherical, with sizes ranging from $24\text{--}30\text{ nm}$.

The electrical conductivity values of BEP and the BEP–Au composites, as determined using a four-point probe at ambient RT , were found to be equal to 6.211 and $9.319 \cdot 10^{-7}\text{ S/cm}$, respectively, (Table 1). After doping the samples with H_2S gas (20 ppm), the conductivity of BEP increased up to $1.530 \cdot 10^{-6}\text{ S/cm}$, which was 2.46-fold higher than that of the undoped sample. Similarly, the conductivity of the doped BEP–Au sensor substantially increased by 21.6-fold to $2.02 \cdot 10^{-5}\text{ S/cm}$. Thus, the conductivity of the doped BEP–Au sensor was 13.2-fold higher than that of the BEP sensor in the doped state.

The cyclic voltammograms of the blank ITO and the ITO coated with BEP and BEP–Au thin films are depicted in Figure 4a. The CV of BEP and the BEP–Au thin films showed a pair of redox peaks at 505 and 559 mV , respectively, which could be attributed to the transition from the emeraldine oxidation state to the pernigraniline oxidation state. Moreover, the current density of the BEP–Au thin films ($9.48\text{ }\mu\text{A/cm}^2$) was fourfold higher than that of BEP ($2.34\text{ }\mu\text{A/cm}^2$). Data on the weight loss of BEP and the BEP–Au thin films in PBS are shown in Figure 4b. The degradation

Table 1. Conductivity data of BEP and BEP–Au samples determined via the four-point probe.

Sample	Un-doped [S/cm]	Doped [S/cm]
BEP	$6.211 \cdot 10^{-7}$	$1.530 \cdot 10^{-6}$
BEP–Au	$9.319 \cdot 10^{-7}$	$2.027 \cdot 10^{-5}$

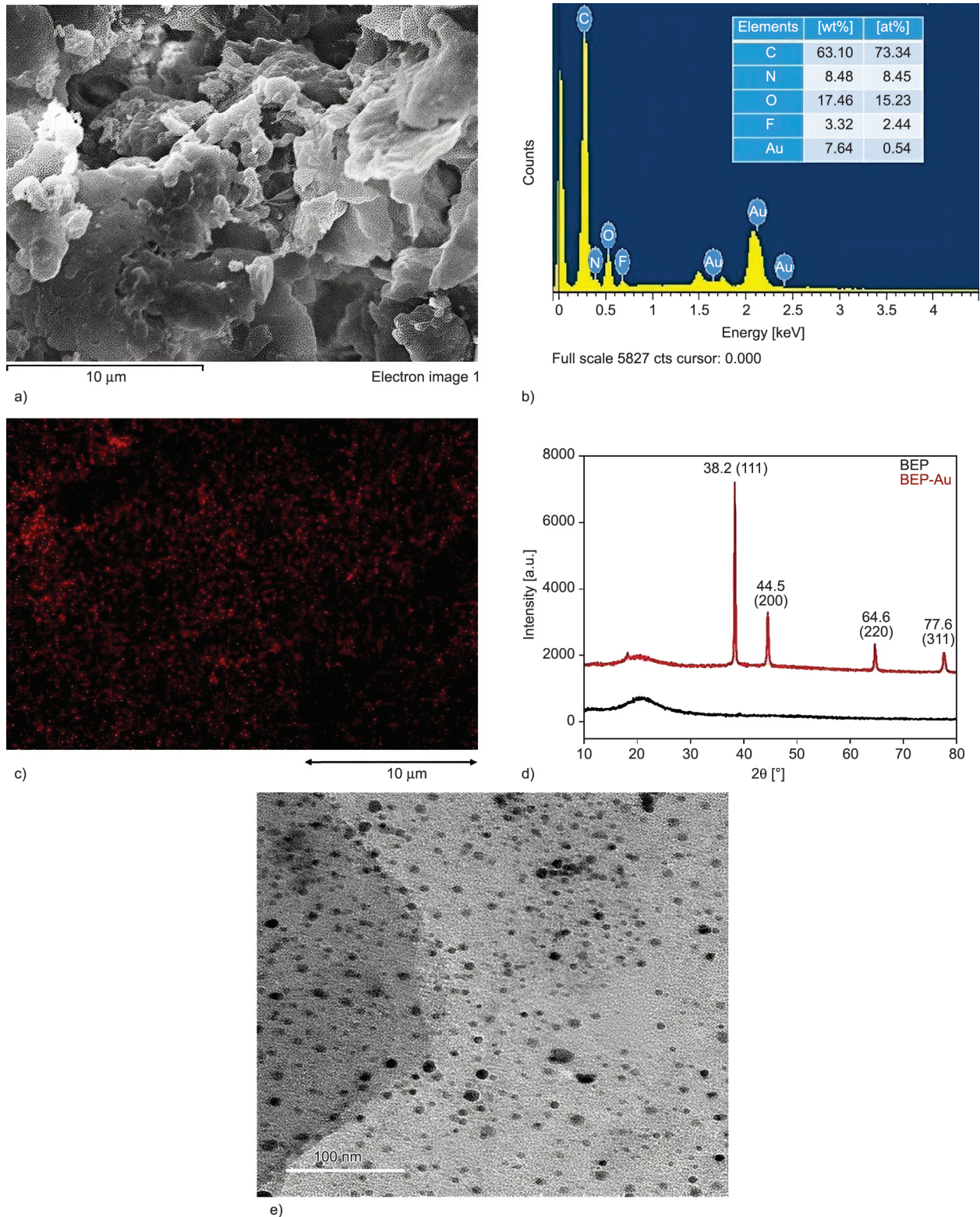


Figure 3. (a) SEM electron image of BEP-Au composite (b) EDX spectrum of BEP-Au composite (c) distribution of Au nanoparticles (d) XRD patterns of BEP and BEP-Au composite, and (e) TEM image of BEP-Au composite.

kinetics of BEP was considerably faster than that of the BEP–Au composites. The first 7 day degradation period did not substantially affect weight loss. However, the degradation period from days 7 to 28

significantly decreased the mass loss ($p < 0.05$). Over a period of 28 days, the biodegradation of BEP was 69%, whereas that of the BEP–Au composites was only 27%.

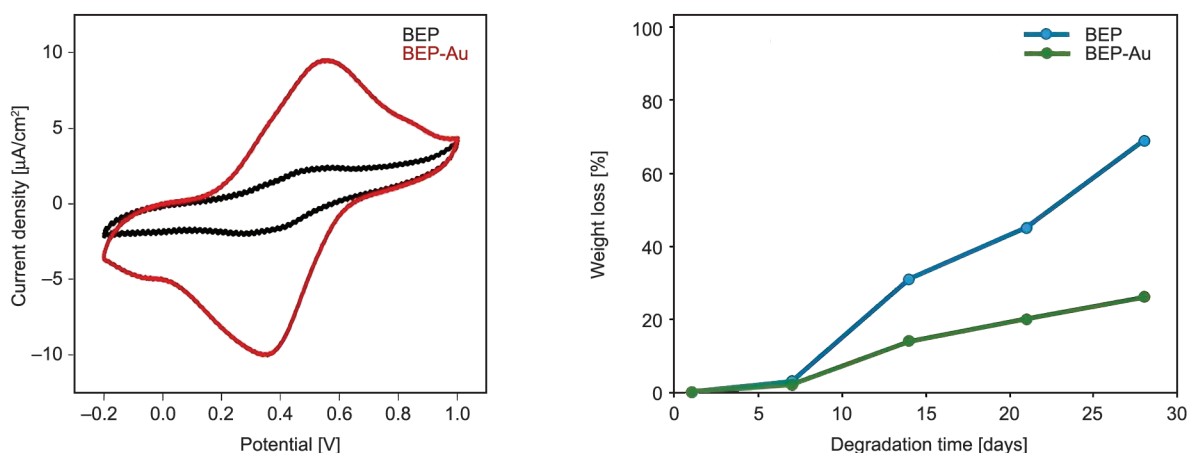


Figure 4. (a) Cyclic voltammograms of BEP and BEP-Au composites in 1 M H_2SO_4 , (b) degradation profile of BEP and BEP-Au films in PBS (pH = 7.4) at 37 °C.

3.2. Gas sensing properties

3.2.1. Response and sensitivity

The sensing performance of the as-synthesized thin films, spin-coated to an ITO electrode, was evaluated by detecting the corresponding changes in their electrical conductivity upon exposure to H_2S gas (1–20 ppm) at 60% RH. Figure 5a shows the variation of the normalized current (I/I_0) as a function of time

for BEP and the BEP-Au thin films at room temperature. The response behaviors of the sensor with and without Au-NPs were markedly different. The observed response values of the BEP sensor were 0.275, 0.35, 0.4, and 0.5 at the corresponding gas concentrations of 1, 5, 10, and 20 ppm, respectively (Figure 5a). Under the same conditions, the BEP-Au sensor had response values of 1.53, 4.62, 10.598,

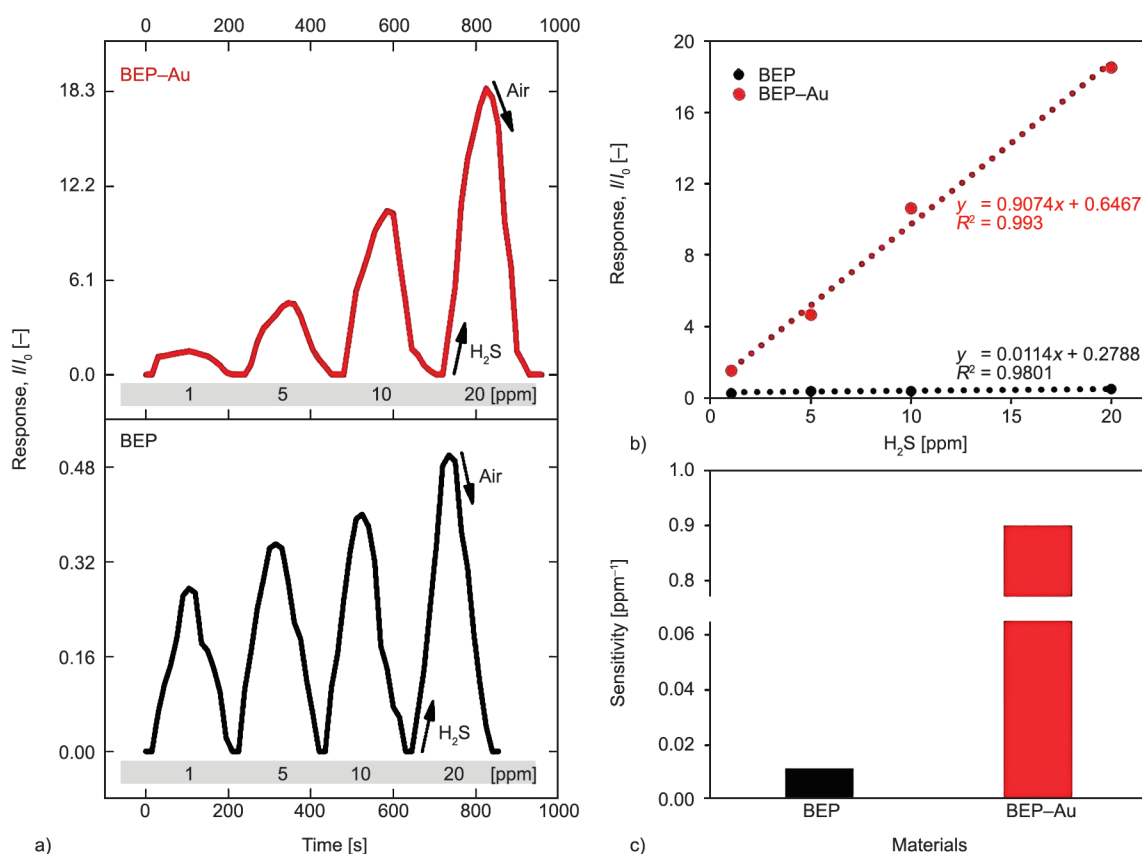


Figure 5. Comparison of the BEP and BEP-Au sensors' performance: (a) dynamic sensing responses upon exposure to H_2S gas with concentration varying from 1 to 20 ppm (1000 sccm, $V = +1$ V, 60% RH) at RT, (b) calibration curves: Response variations as a function of H_2S concentration ($V = +1$ V), (c) sensitivity values.

and 18.5 to H₂S gas concentration ranging from 1–20 ppm. On average, the response of the BEP–Au sensor was 20-fold times higher than that of the BEP sensor.

The BEP–Au sensor had a higher gas response compared to the BEP sensor. This enhanced gas response could be due to the high catalytic activity of Au NPs, as evidenced by the dramatic 20-fold increase in the conductivity of the BEP–Au sensor upon exposure to H₂S gas. The linear calibration curve in Figure 5b shows the response of these BEP and BEP–Au sensors as a function of H₂S concentration. The linear fitting equations were $y = 0.0114x + 0.2788$ and $y = 0.9074x + 0.6467$ for the BEP and BEP–Au sensors, respectively. The correlation coefficients of the fitted data (R^2) were 0.9801 and 0.993, respectively. Moreover, the sensor's sensitivity (S , [ppm⁻¹]) was calculated as the slope of the normalized sensor response I/I_0 (Figure 5c). The sensitivity of the BEP and BEP–Au sensors was 0.114 and 0.9074 ppm⁻¹, respectively.

Noble metals are often used as sensitizing agents in gas sensors as they provide additional adsorption sites and promote chemical reactions on the surface. They tend to increase the gas response in two ways.

First, Au-NPs facilitated material–gas interaction as they have a high affinity for analytes containing sulfur atoms, such as H₂S. In fact, H₂S gas reacted with Au to form AuS and H⁺, thereby enhancing the doping of BEP polymer that, in turn, increased the sensor's response. Second, the presence of Au-NPs in BEP

induced the formation of nano-Schottky junctions (Figure 6), which might have amplified the sensor's response towards H₂S gas, resulting in enhanced response [67].

3.2.2. Response/recovery time

The dynamic response/recovery time of the BEP and BEP–Au sensors as a function of H₂S gas concentration is shown in Figure 7. On the one hand, the quick response time (dashed line) of the BEP sensor decreased from 30 to 15 s (± 0.05) as H₂S gas concentration increased from 1 to 20 ppm. By contrast, the response time of the BEP–Au sensor decreased from 20 to 1 s as H₂S gas concentration increased from 1 to 20 ppm. The quick response time of the BEP–Au sensor may be attributed to the presence of Au NPs that endowed the sensor with high sensitivity with more adsorption sites. On the other hand, the recovery time (solid line) of the composite ranged from 80 to 150 s (Figure 7a).

At 20 ppm of H₂S gas, the BEP–Au sensor had the longest recovery time of 150 s (± 0.05) compared with the BEP sensor, which had a recovery time of 90 s only. The relatively long recovery time of the BEP–Au sensor might be due to the high affinity of the composite sensor to H₂S gas, leading to a lower desorption rate compared with the adsorption rate.

3.2.3. Stability

The stability of the as-prepared sensors was tested via repeated experiments on their gas-sensing performance to 20 ppm H₂S at room temperature. Figure 7b shows their stability values *versus* storage time. Their response [%] decreased over time because the sensitivity ratio of the BEP sensor was considerably faster than that of the BEP–Au sensor. The total degradation time of the BEP sensor was 192 h, whereas that of the BEP–Au sensor was 480 h or 20 days.

3.2.4. Selectivity

Selectivity is an important performance indicator of the reliability of a gas sensor. The BEP and BEP–Au sensors were exposed to various gases, including H₂S, SO₂, NH₃, NO₂, CO, and CO₂ at 20 ppm at room temperature. Figure 7c shows the response values of all sensors to different gases. The BEP–Au sensor had the highest response value to H₂S compared with the other test gases. Moreover, its response to H₂S, as opposed to other gases, was evidently better than that of the BEP sensor. Thus, the BEP–Au sensor showed

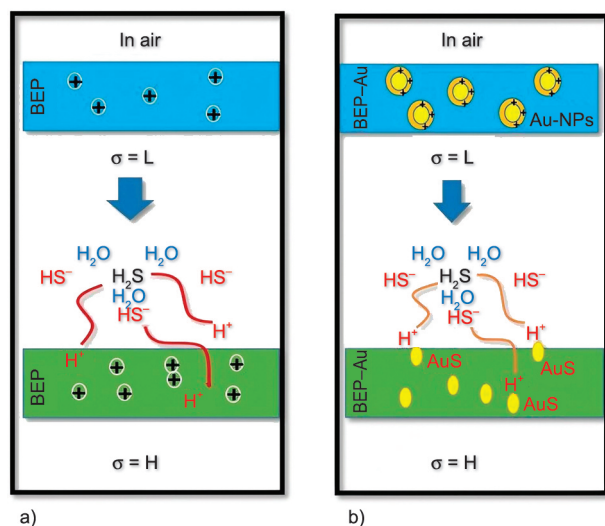


Figure 6. Mechanism of H₂S gas sensing by (a) BEP and (b) BEP composite with gold nanoparticles (Au-NPs) where σ represents the conductivity, which tend to increase as the polymer film comes in contact with H₂S. (Adapted from [67]).

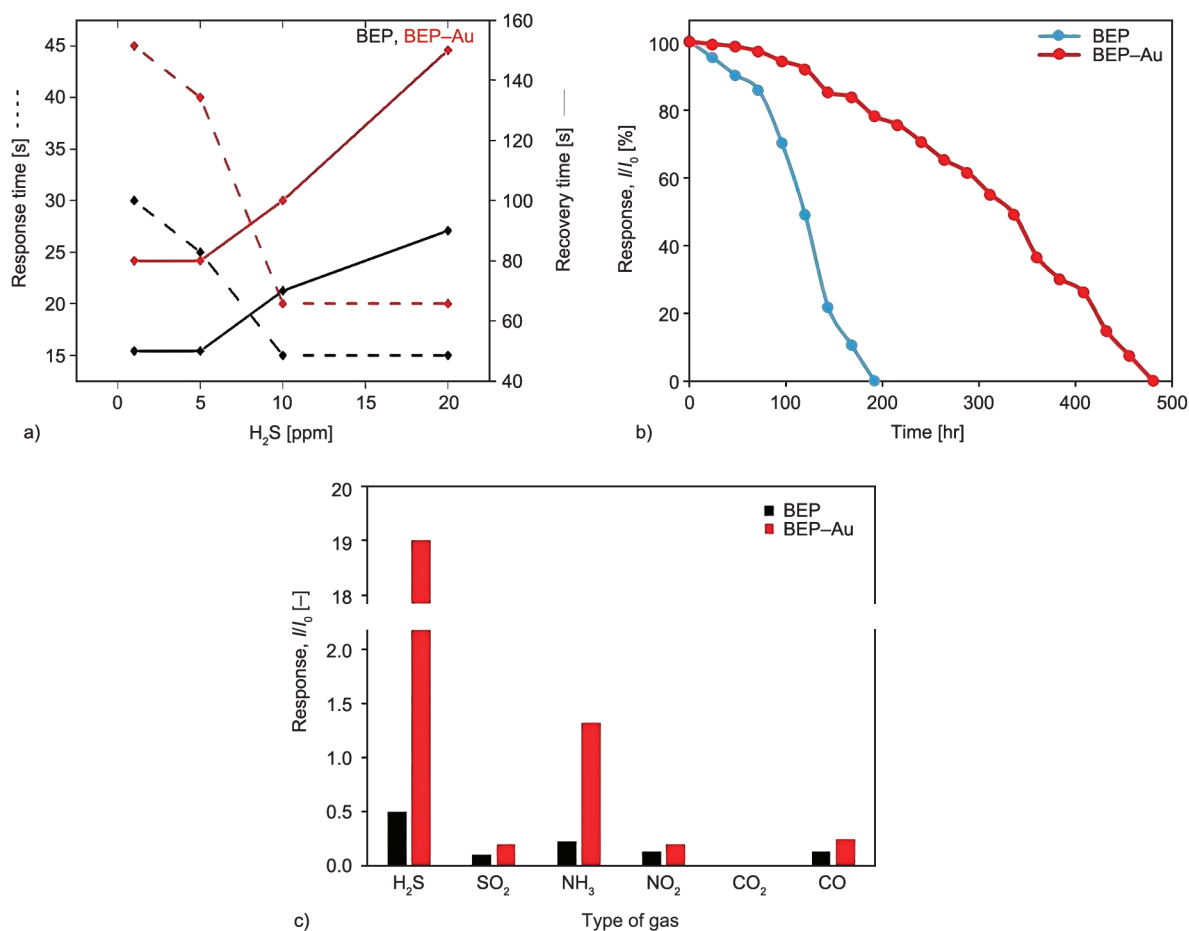


Figure 7. (a) Response time (---) and recovery time (—) of BEP and BEP-Au sensors at different H₂S gas concentrations from 1 to 20 ppm at RT. (b) Stability of BEP and BEP-Au sensors exposed to 20 ppm H₂S gas at RT tested over 480 h. (c) Detection selectivity of BEP and BEP-Au gas sensor upon exposure to various gases (20 ppm) at RT.

excellent selectivity to H₂S against other gases at room temperature.

3.2.5. Repeatability

Repeatability is another parameter that indicates a sensor's performance. Five consecutive responses were measured at room temperature by exposing the BEP and BEP-Au sensors to H₂S gas at 20 ppm. The sensors showed excellent repeatability with almost identical curves (Figure 8). The BEP (Figure 8a) and BEP-Au (Figure 8b) sensors displayed a stable response with values of 0.46 ± 0.0008 and 18.5 ± 0.0046 , respectively.

3.3. Gas sensing mechanism

Like polyaniline [68, 69], most of the charge carriers present in BEP are holes; thus, it is also a *p*-type semiconductor. When it was exposed to reducing gases, such as H₂S, its electrical conductivity changed because of adsorption and desorption on the surface of the BEP and BEP-Au films. Thus, H₂S possibly

interacted with BEP through this pathway (Equations (5) and (6)) [10, 68]:



In addition to the doping effect previously mentioned, the other functional groups in BEP may also have contributed and played a role in gas sensing activity. The hydroxyl group can strongly interact with polar H₂S and other oxygen-containing functional groups due to the formation of intermolecular forces of attraction such as H-bonding, dipole-dipole, and electrostatic interactions [10] as shown in Figure 9. The *ab initio* DFT calculations included adsorption energy (E_{ads}), charge transfer (e^-), and recovery time (τ) for different adsorption sites (Table 2).

Figure 10 shows the adsorption energies of pure ACAT (Figures 10a and 10b) and PLA (Figure 10c). The H₂S adsorption energies of pristine ACAT

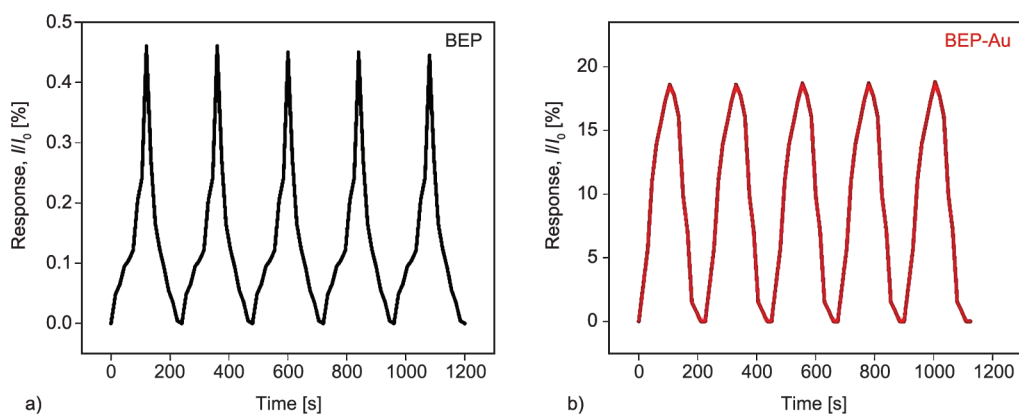


Figure 8. Repeatability test of BEP (a) and BEP–Au (b) sensor upon exposure to 20 ppm of H₂S gas flowed through the measuring chamber (1000 sccm, $V = +1$ V, 60% RH) at RT.

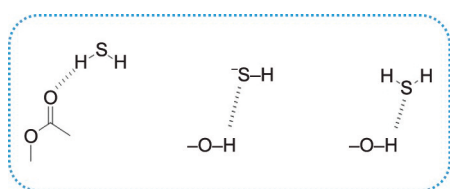


Figure 9. Electrostatic interactions pathway between oxygen-containing functional groups group and H₂S.

(−0.161 and −0.166 eV) and PLA (−0.122 eV) are also shown in Figure 10.

The inclusion of Au into the ACAT system increased the adsorption energy to −0.828 and −0.826 eV (Figures 10d and 10e). Site *d* and site *e* had higher adsorption energy, which corresponded to their highest adsorption energy value and the shortest adsorbent–

Table 2. Adsorption energies, Mulliken charges and recovery time of H₂S on various configurations.

System	E_{ads} [kJ/mol]	Mulliken charge for H ₂ S [e ⁻]	Bond Angle of H ₂ S [°]	Recovery time [s]
ACAT+H ₂ S (site <i>a</i>)	−0.161	−0.006	93.039	$5.27 \cdot 10^{14}$
ACAT+H ₂ S (site <i>b</i>)	−0.166	−0.019	93.052	$6.40 \cdot 10^{14}$
PLA+H ₂ S (site <i>c</i>)	−0.122	0.020	93.026	$1.16 \cdot 10^{14}$
ACAT+Au+H ₂ S (site <i>d</i>)	−0.828	0.573	93.329	$9.97 \cdot 10^{25}$
ACAT+Au+H ₂ S (site <i>e</i>)	−0.826	0.566	93.300	$9.23 \cdot 10^{25}$

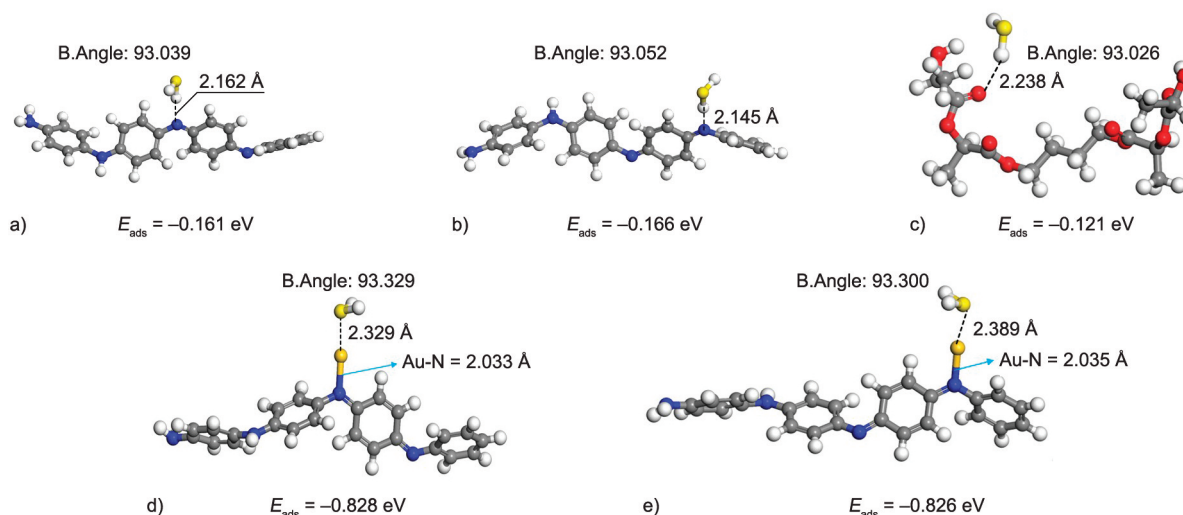


Figure 10. Molecular models showing the adsorption sites of H₂S on electroactive ACAT (a, b), biodegradable PLA (c), and ACAT doped with Au NPs (d, e). The atoms are presented using the following color assignment: yellow ● – S, grey ● – C, red ● – O, blue ● – N, white ○ – H and golden ● – Au.

adsorbate distance. Thus, they performed better for H₂S sensing. The DFT calculations revealed that the interaction between ACAT+Au and H₂S involved strong bonds with a predicted Au–N and Au–S bond distance of 2.03/2.33 and 2.04/2.39 Å, respectively. Site *d* and site *e* had corresponding adsorption energies (E_{ads}) of -0.828 and -0.826 eV, respectively, which were stronger than those of pure ACAT.

This result demonstrated that the structure incorporated with Au had a better gas sensing performance than pure ACAT. Mulliken population analysis revealed that more electrons were transferred from H₂S to ACAT+Au ($+0.573$ |e| for site *d* and $+0.566$ |e| for site *e*), indicating that H₂S played the role of an electron donor (Table 2). Furthermore, the recovery time of the ACAT (Figures 10a and 10b), PLA (Figure 10c), and ACAT+Au (Figures 10d and 10e) systems was 5.27, 6.40, 1.16, 9.97 and $9.23 \cdot 10^{25}$ s, respectively. According to Equation (3), the enhancement in E_{ads} led to an increase in recovery time and stronger interactions between H₂S molecules and ACAT systems. Furthermore, according to the results of the analysis of recovery time, the high negative E_{ads} value led to a long desorption time of H₂S gas molecules from ACAT. Therefore, the ACAT+Au system had a higher sensitivity towards H₂S gas molecules than the pristine ACAT system. According to the computational results, the adsorption energy and recovery time of the ACAT+Au (Figures 10d and 10e) were considerably larger than those of ACAT (Figures 10a and 10b), indicating that the incorporation of Au substantially promoted the gas-sensing performance of ACAT, in agreement with the experimental results.

4. Conclusions

In this study, we successfully developed and characterized H₂S gas sensors based on BEP and its nanocomposite with Au-NPs (BEP–Au). BEP, which has a biodegradable backbone made of PLA and ACAT as an electroactive part, was found to have a pendant group. The monomers and polymers were characterized via ion-trap mass spectrometry, GPC, FTIR, NMR, and UV-Vis absorption spectrum analyses that led to interesting results. The presence of Au-NPs was further confirmed via EDX, XRD, and TEM. The size and morphological distribution of the NPs were determined via TEM. Doping of BEP with Au NPs improved its properties, including its biodegradability,

conductivity, and thermal, electrical, and gas-sensing properties. The conductivity of the as-prepared samples was determined by doping thin films with H₂S gas at 20 ppm and a ratio of 13.2:1. Over a period of 28 days, the BEP sensor had a considerably higher degradation rate of 73% than the BEP–Au sensor (37%). The current density of the BEP–Au sensor was $9.48 \mu\text{A}/\text{cm}^2$, which was four-fold higher than that of the BEP sensor ($2.34 \mu\text{A}/\text{cm}^2$). The gas-sensing performance of the sensors was determined by measuring various parameters, including their response rate, sensitivity, selectivity, stability, and repeatability. The BEP–Au sensor showed a good sensitivity towards H₂S gas concentration ranging from 1 to 20 ppm at room temperature. The BEP–Au sensor had a response rate that was 20-fold higher than that of the BEP sensors. This result was also confirmed by DFT calculations. The adsorption mechanism of the sensors was investigated in terms of adsorption energy and charge transfer. The adsorption structures of the H₂S molecules on the Au-doped BEP sensor with larger adsorption energies were stable and had a higher charge transfer than the corresponding BEP adsorption structure. The BEP–Au sensor showed long-term stability with a lifetime of 480 h or 20 days, whereas the BEP sensor had a life span of 192 h or 8 days only. This difference in life span could be attributed to the biodegradable nature of BEP. Moreover, the BEP and BEP–Au sensors exhibited an average fast response of 15–45 s, good reproducibility, and a short recovery time of 50–150 s, indicating their promising application as gas-sensing materials. Thus, the BEP and BEP–Au gas sensors could be a good candidate for sensing H₂S gas at room temperature.

Acknowledgements

This research was funded by the Ministry of Science and Technology, Taiwan, R.O.C through (MOST 109-2113-M-033-002-), department of chemistry, center for nanotechnology, center for membrane technology and R & D center for biomedical technology at CYCU.

References

- [1] Jeon J-W., Ma Y., Mike J. F., Shao L., Balbuena P. B., Lutkenhaus J. L.: Oxidatively stable polyaniline:polyacid electrodes for electrochemical energy storage. *Physical Chemistry Chemical Physics*, **15**, 9654–9662 (2013). <https://doi.org/10.1039/C3CP51620B>

- [2] Dhand C., Dwivedi N., Mishra S., Solanki P., Mayadi V., Beuerman R. W., Ramakrishna S., Lakshminarayanan R., Malhotra B.: Polyaniline-based biosensors. Nano-biosensors in Disease Diagnosis, **2015**, 25–46 (2015). <https://doi.org/10.2147/NDD.S64841>
- [3] Gvozdenović M., Jugović B., Jambrec D., Stevanović J., Grgur B. N.: Application of polyaniline in corrosion protection of metals. *Zaštita Materijala*, **53**, 353–360 (2012).
- [4] Wang H., Lin J., Shen Z. X.: Polyaniline (PANi) based electrode materials for energy storage and conversion. *Journal of Science: Advanced Materials and Devices*, **1**, 225–255 (2016). <https://doi.org/10.1016/j.jsamd.2016.08.001>
- [5] Bai H., Shi G.: Gas sensors based on conducting polymers. *Sensors*, **7**, 267–307 (2007). <https://doi.org/10.3390/s7030267>
- [6] Gautam S. K., Panda S.: Effect of moisture and molecular weight of polyaniline on H₂S sensing characteristics. *Sensors and Actuators B: Chemical*, **344**, 130323 (2021). <https://doi.org/10.1016/j.snb.2021.130323>
- [7] Reddy A., Patil N., Bolegaon N. N.: Fabrication, characterization, and gas sensing properties of CaMnO₃ doped polyaniline nano composite thin films. *ECS Transactions*, **107**, 11467–11477 (2022). <https://doi.org/10.1149/10701.11467ecst>
- [8] Zuo P., Wang R., Li F., Wu F., Xu G., Niu W.: A trace ppb-level electrochemical H₂S sensor based on ultrathin Pt nanotubes. *Talanta*, **233**, 122539 (2021). <https://doi.org/10.1016/j.talanta.2021.122539>
- [9] Beygisangchin M., Rashid S., Shafie S. A., Sadrolhosseini A. R., Lim H. N.: Preparations, properties, and applications of polyaniline and polyaniline thin films – A review. *Polymers*, **13**, 2003 (2021). <https://doi.org/10.3390/polym13122003>
- [10] Bibi A., Huang C-H., Lan Y-X., Chen K-Y., Ji W-F., Yeh J-M., Santiago K. S.: Effect of surface morphology of electro-spun EPAA coatings on the H₂S sensing performance of corresponding interdigitated electrodes. *Journal of The Electrochemical Society*, **167**, 117510 (2020). <https://doi.org/10.1149/1945-7111/aba933>
- [11] Guarino V., Zuppolini S., Borriello A., Ambrosio L.: Electro-active polymers (EAPs): A promising route to design bio-organic/bioinspired platforms with on demand functionalities. *Polymers*, **8**, 185 (2016). <https://doi.org/10.3390/polym8050185>
- [12] Udeh C. U., Fey N., Faul C. F. J.: Functional block-like structures from electroactive tetra(aniline) oligomers. *Journal of Materials Chemistry*, **21**, 18137–18153 (2011). <https://doi.org/10.1039/C1JM12557E>
- [13] Wei Z., Faul C. F. J.: Aniline oligomers – Architecture, function and new opportunities for nanostructured materials. *Macromolecular Rapid Communications*, **29**, 280–292 (2008). <https://doi.org/10.1002/marc.200700741>
- [14] Shumakovich G. P., Otrokhov G. V., Khlupova M. E., Vasil'Eva I. S., Zaitseva E. A., Morozova O. V., Yaropolov A. I.: Laccase-catalyzed synthesis of aniline oligomers and their application for the protection of copper against corrosion. *RSC Advances*, **4**, 30193–30196 (2014). <https://doi.org/10.1039/C4RA04836A>
- [15] Yang F., Liu Y., Liu T., Liu S., Zhao H.: Aniline trimer-including carboxymethylated β-cyclodextrin as an efficient corrosion inhibitor for Q235 carbon steel in 1 M HCl solution. *RSC Advances*, **9**, 30249–30258 (2019). <https://doi.org/10.1039/C9RA04047A>
- [16] Ye Y., Zhao H., Wang C., Zhang D., Chen H., Liu W.: Design of novel superhydrophobic aniline trimer modified siliceous material and its application for steel protection. *Applied Surface Science*, **457**, 752–763 (2018). <https://doi.org/10.1016/j.apsusc.2018.06.135>
- [17] Bagher Z., Atoufi Z., Alizadeh R., Farhadi M., Zarrintaj P., Moroni L., Setayeshmehr M., Komeili A., Kamrava S. K.: Conductive hydrogel based on chitosan-aniline pentamer/gelatin/agarose significantly promoted motor neuron-like cells differentiation of human olfactory ectomesenchymal stem cells. *Materials Science and Engineering C*, **101**, 243–253 (2019). <https://doi.org/10.1016/j.msec.2019.03.068>
- [18] Tsai M-H., Lu S-H., Lai Y-H., Lai G-H., Dizon G. V., Yang T-I., Lin Y-J., Chou Y. C.: Novel ascorbic acid sensor prepared from gold-aniline pentamer-based electroactive polyamide composite. *eXpress Polymer Letters*, **12**, 71–81 (2018). <https://doi.org/10.3144/expresspolymlett.2018.6>
- [19] Bibi A., Hsu S-C., Ji W-F., Cho Y-C., Santiago K. S., Yeh J-M.: Comparative studies of CPEs modified with distinctive metal nanoparticles decorated electroactive polyimide for the detection of UA. *Polymer*, **13**, 252 (2021). <https://doi.org/10.3390/polym13020252>
- [20] Lindino C. A., Casagrande M., Peiter A., Ribeiro C.: Poly(*o*-methoxyaniline) modified electrode for detection of lithium ions. *Quimica Nova*, **35**, 449–453 (2012). <https://doi.org/10.1590/S0100-40422012000300002>
- [21] Zhao B., Sai T., Rahman A., Levon K.: Floating-gate ion sensitive field-effect transistor for chemical and biological sensing. *MRS Online Proceedings Library*, **828**, 349–354 (2004). <https://doi.org/10.1557/PROC-828-A7.8>
- [22] Gupta A. P., Kumar V.: New emerging trends in synthetic biodegradable polymers – Polylactide: A critique. *European Polymer Journal*, **43**, 4053–4074 (2007). <https://doi.org/10.1016/j.eurpolymj.2007.06.045>
- [23] Ibrahim M. S., Sani N., Adamu M., Abubakar M. K.: Biodegradable polymers for sustainable environmental and economic development. *MOJ Bioorganic & Organic Chemistry*, **2**, 192–194 (2018). <https://doi.org/10.15406/mojboc.2018.02.00080>
- [24] Vroman I., Tighzert L.: Biodegradable polymers. *Materials*, **2**, 307–344 (2009). <https://doi.org/10.3390/ma2020307>

- [25] Raquez J-M., Habibi Y., Murariu M., Dubois P.: Polylactide (PLA)-based nanocomposites. *Progress in Polymer Science*, **38**, 1504–1542 (2013).
<https://doi.org/10.1016/j.progpolymsci.2013.05.014>
- [26] Wang G., Zhao G., Wang S., Zhang L., Park C. B.: Injection-molded microcellular PLA/graphite nanocomposites with dramatically enhanced mechanical and electrical properties for ultra-efficient EMI shielding applications. *Journal of Materials Chemistry C*, **6**, 6847–6859 (2018).
<https://doi.org/10.1039/C8TC01326H>
- [27] Wang G., Wang L., Mark L. H., Shaayegan V., Wang G., Li H., Zhao G., Park C. B.: Ultralow-threshold and lightweight biodegradable porous PLA/MWCNT with segregated conductive networks for high-performance thermal insulation and electromagnetic interference shielding applications. *ACS Applied Materials and Interfaces*, **10**, 1195–1203 (2018).
<https://doi.org/10.1021/acsami.7b14111>
- [28] Lee G., Kang S-K., Won S. M., Gutruf P., Jeong Y. R., Koo J., Lee S-S., Rogers J. A., Ha J. S.: Fully biodegradable microsupercapacitor for power storage in transient electronics. *Advanced Energy Materials*, **7**, 1700157 (2017).
<https://doi.org/10.1002/aenm.201700157>
- [29] Ivanov E., Kotsilkova R., Xia H., Chen Y., Donato R. K., Donato K., Godoy A. P., Di Maio R., Silvestre C., Cimmino S., Angelov V.: PLA/graphene/MWCNT composites with improved electrical and thermal properties suitable for FDM 3D printing applications. *Applied Sciences MDPI*, **9**, 1209 (2019).
<https://doi.org/10.3390/app9061209>
- [30] Abdalhadi D. M., Abbas Z., Ahmad A. F., Matori K. A., Esa F.: Controlling the properties of OPEFB/PLA polymer composite by using Fe₂O₃ for microwave applications. *Fibers and Polymers*, **19**, 1513–1521 (2018).
<https://doi.org/10.1007/s12221-018-8118-y>
- [31] Yuryev Y., Mohanty A. K., Misra M.: Novel biocomposites from biobased PC/PLA blend matrix system for durable applications. *Composites Part B: Engineering*, **130**, 158–166 (2017).
<https://doi.org/10.1016/j.compositesb.2017.07.030>
- [32] Marasso S. L., Cocuzza M., Bertana V., Perrucci F., Tommasi A., Ferrero S., Scaltrito L., Pirri C. F.: PLA conductive filament for 3D printed smart sensing applications. *Rapid Prototyping Journal*, **24**, 739–743 (2018).
<https://doi.org/10.1108/RPJ-09-2016-0150>
- [33] Luo M., Martinez A. W., Song C., Herrault F., Allen M. G.: A microfabricated wireless RF pressure sensor made completely of biodegradable materials. *Journal of Microelectromechanical Systems*, **23**, 4–13 (2014).
<https://doi.org/10.1109/JMEMS.2013.2290111>
- [34] Mallick S., Ahmad Z., Touati F., Bhadra J., Shakoor R. A., Al-Thani N. J.: PLA-TiO₂ nanocomposites: Thermal, morphological, structural, and humidity sensing properties. *Ceramics International*, **44**, 16507–16513 (2018).
<https://doi.org/10.1016/j.ceramint.2018.06.068>
- [35] Katseli V., Economou A., Kokkinos C.: Single-step fabrication of an integrated 3D-printed device for electrochemical sensing applications. *Electrochemistry Communications*, **103**, 100–103 (2019).
<https://doi.org/10.1016/j.elecom.2019.05.008>
- [36] Silva V. A. O. P., Fernandes-Junior W. S., Rocha D. P., Stefano J. S., Munoz R. A. A., Bonacin J. A., Janegitz B. C.: 3D-printed reduced graphene oxide/polylactic acid electrodes: A new prototyped platform for sensing and biosensing applications. *Biosensors and Bioelectronics*, **170**, 112684 (2020).
<https://doi.org/10.1016/j.bios.2020.112684>
- [37] Zhang B. L., Yang Y., Zhao Z. Q., Guo X. D.: A gold nanoparticles deposited polymer microneedle enzymatic biosensor for glucose sensing. *Electrochimica Acta*, **358**, 136917 (2020).
<https://doi.org/10.1016/j.electacta.2020.136917>
- [38] Sathies T., Senthil P., Prakash C.: Application of 3D printed PLA-carbon black conductive polymer composite in solvent sensing. *Materials Research Express*, **6**, 115349 (2019).
<https://doi.org/10.1088/2053-1591/ab5040>
- [39] Kumar B., Castro M., Feller J. F.: Poly(lactic acid)-multi-wall carbon nanotube conductive biopolymer nanocomposite vapour sensors. *Sensors and Actuators, B: Chemical*, **161**, 621–628 (2012).
<https://doi.org/10.1016/j.snb.2011.10.077>
- [40] Xu C., Huang Y., Yopez G., Wei Z., Liu F., Bugarin A., Tang L., Hong Y.: Development of dopant-free conductive bioelastomers. *Scientific Reports*, **6**, 34451 (2016).
<https://doi.org/10.1038/srep34451>
- [41] Xie M., Wang L., Ge J., Guo B., Ma P. X.: Strong electroactive biodegradable shape memory polymer networks based on star-shaped polylactide and aniline trimer for bone tissue engineering. *ACS Applied Materials and Interfaces*, **7**, 6772–6781 (2015).
<https://doi.org/10.1021/acsami.5b00191>
- [42] Guo B., Finne-Wistrand A., Albertsson A. C.: Molecular architecture of electroactive and biodegradable copolymers composed of polylactide and carboxyl-capped aniline trimer. *Biomacromolecules*, **11**, 855–863 (2010).
<https://doi.org/10.1021/bm9011248>
- [43] Hardy J. G., Mouser D. J., Arroyo-Currás N., Geissler S., Chow J. K., Nguy L., Kim J. M., Schmidt C. E.: Biodegradable electroactive polymers for electrochemically-triggered drug delivery. *Journal of Materials Chemistry B*, **2**, 6809–6822 (2014).
<https://doi.org/10.1039/C4TB00355A>
- [44] Liu Y., Hu J., Zhuang X., Zhang P., Wei Y., Wang X., Chen X.: Synthesis and characterization of novel biodegradable and electroactive hydrogel based on aniline oligomer and gelatin. *Macromolecular Bioscience*, **12**, 241–250 (2012).
<https://doi.org/10.1002/mabi.201100227>

- [45] Cui H., Wang Y., Cui L., Zhang P., Wang X., Wei Y., Chen X.: *In vitro* studies on regulation of osteogenic activities by electrical stimulus on biodegradable electroactive polyelectrolyte multilayers. *Biomacromolecules*, **15**, 3146–3157 (2014).
<https://doi.org/10.1021/bm5007695>
- [46] Gautam V., Singh K. P., Yadav V. L.: Preparation and characterization of green-nano-composite material based on polyaniline, multiwalled carbon nano tubes and carboxymethyl cellulose: For electrochemical sensor applications. *Carbohydrate Polymers*, **189**, 218–228 (2018).
<https://doi.org/10.1016/j.carbpol.2018.02.029>
- [47] Macagnano A., Perri V., Zampetti E., Bearzotti A., De Cesare F.: Humidity effects on a novel eco-friendly chemosensor based on electrospun PANi/PHB nanofibres. *Sensors and Actuators B: Chemical*, **232**, 16–27 (2016).
<https://doi.org/10.1016/j.snb.2016.03.055>
- [48] Kruefu V., Wisitsoraat A., Tuantranont A., Phanichphant S.: Gas sensing properties of conducting polymer/Au-loaded ZnO nanoparticle composite materials at room temperature. *Nanoscale Research Letters*, **9**, 467 (2014).
<https://doi.org/10.1186/1556-276X-9-467>
- [49] Jiang S., Chen J., Tang J., Jin E., Kong L., Zhang W., Wang C.: Au nanoparticles-functionalized two-dimensional patterned conducting PANI nanobowl monolayer for gas sensor. *Sensors and Actuators B: Chemical*, **140**, 520–524 (2009).
<https://doi.org/10.1016/j.snb.2009.04.060>
- [50] Chang Q., Zhao K., Chen X., Li M., Liu J.: Preparation of gold/polyaniline/multiwall carbon nanotube nanocomposites and application in ammonia gas detection. *Journal of Materials Science*, **43**, 5861–5866 (2008).
<https://doi.org/10.1007/s10853-008-2827-3>
- [51] Chen L., Yu Y., Mao H., Lu X., Zhang W., Wei Y.: Synthesis of parent aniline tetramer and pentamer and redox properties. *Materials Letters*, **59**, 2446–2450 (2005).
<https://doi.org/10.1016/j.matlet.2005.03.018>
- [52] Weng C-J., Hsu P-H., Hsu S-C., Chang C-H., Hung W-I., Wu P-S., Yeh J-M.: Synthesis of electroactive mesoporous gold-organosilica nanocomposite materials *via* a sol-gel process with non-surfactant templates and the electroanalysis of ascorbic acid. *Journal of Materials Chemistry B*, **1**, 4983–4991 (2013).
<https://doi.org/10.1039/C3TB20433B>
- [53] Baheiraei N., Yeganeh H., Ai J., Gharibi R., Azami M., Faghihi F.: Synthesis, characterization and antioxidant activity of a novel electroactive and biodegradable polyurethane for cardiac tissue engineering application. *Materials Science and Engineering C*, **44**, 24–37 (2014).
<https://doi.org/10.1016/j.msec.2014.07.061>
- [54] Chen Q-Z., Bismarck A., Hansen U., Junaid S., Tran M. Q., Harding S. E., Ali N. N., Boccaccini A. R.: Characterisation of a soft elastomer poly(glycerol sebacate) designed to match the mechanical properties of myocardial tissue. *Biomaterials*, **29**, 47–57 (2008).
<https://doi.org/10.1016/j.biomaterials.2007.09.010>
- [55] Crowley K., Morrin A., Shepherd R. L., in het Panhuis M., Wallace G. G., Smyth M. R., Killard A. J.: Fabrication of polyaniline-based gas sensors using piezoelectric inkjet and screen printing for the detection of hydrogen sulfide. *IEEE Sensors Journal*, **10**, 1419–1426 (2010).
<https://doi.org/10.1109/JSEN.2010.2044996>
- [56] Gaikwad G., Patil P., Patil D., Naik J.: Synthesis and evaluation of gas sensing properties of PANI based graphene oxide nanocomposites. *Materials Science and Engineering B*, **218**, 14–22 (2017).
<https://doi.org/10.1016/j.mseb.2017.01.008>
- [57] Mekki A., Joshi N., Singh A., Salmi Z., Jha P., Decorse P., Lau-Truong S., Mahmoud R., Chehimi M. M., Aswal D. K., Gupta S. K.: H₂S sensing using *in situ* photo-polymerized polyaniline-silver nanocomposite films on flexible substrates. *Organic Electronics*, **15**, 71–81 (2014).
<https://doi.org/10.1016/j.orgel.2013.10.012>
- [58] Patil L. A., Pathan I. G., Suryawanshi D. N., Bari A. R., Rane D. S.: Spray pyrolyzed ZnSnO₃ nanostructured thin films for hydrogen sensing. *Procedia Materials Science*, **6**, 1557–1565 (2014).
<https://doi.org/10.1016/j.mspro.2014.07.137>
- [59] Li Z-F., Blum F. D., Bertino M. F., Kim C-S.: Understanding the response of nanostructured polyaniline gas sensors. *Sensors and Actuators B: Chemical*, **183**, 419–427 (2013).
<https://doi.org/10.1016/j.snb.2013.03.125>
- [60] Becke A. D.: Density functional thermochemistry. III. The role of exact exchange. *The Journal of Chemical Physics*, **98**, 5648–5652 (1993).
<https://doi.org/10.1063/1.464913>
- [61] Hay P. J., Wadt W. R.: *Ab initio* effective core potentials for molecular calculations. potentials for K to Au including the outermost core orbital. *The Journal of Chemical Physics*, **82**, 299–310 (1985).
<https://doi.org/10.1063/1.448975>
- [62] Imanzadeh G., Basharnavaz H., Habibi-Yangjeh A., Kamali S. H.: Adsorption behavior of H₂S on P-doped, V/P, Nb/P, and Ta/P-codoped graphitic carbon nitride: A first-principles investigation. *Materials Chemistry and Physics*, **252**, 123117 (2020).
<https://doi.org/10.1016/j.matchemphys.2020.123117>
- [63] Li M., Chen J., Shi M., Zhang H., Ma P. X., Guo B.: Electroactive anti-oxidant polyurethane elastomers with shape memory property as non-adherent wound dressing to enhance wound healing. *Chemical Engineering Journal*, **375**, 121999 (2019).
<https://doi.org/10.1016/j.cej.2019.121999>
- [64] Farea M. O., Abdelghany A. M., Oraby A. H.: Optical and dielectric characteristics of polyethylene oxide/sodium alginate-modified gold nanocomposites. *RSC Advances*, **10**, 37621–37630 (2020).
<https://doi.org/10.1039/D0RA07601E>

- [65] Chieng B. W., Ibrahim N. A., Yunus W. M. Z. W., Hussein M. Z.: Poly(lactic acid)/poly(ethylene glycol) polymer nanocomposites: Effects of graphene nanoplatelets. *Polymers*, **6**, 93–104 (2014).
<https://doi.org/10.3390/polym6010093>
- [66] Ahn S., Singh P., Jang M., Kim Y.-J., Castro-Aceituno V., Simu S. Y., Kim Y. J., Yang D.-C.: Gold nanoflowers synthesized using *acanthopanax* cortex extract inhibit inflammatory mediators in LPS-induced RAW264.7 macrophages *via* NF- κ B and AP-1 pathways. *Colloids and Surfaces B: Biointerfaces*, **162**, 398–404 (2018).
<https://doi.org/10.1016/j.colsurfb.2017.11.037>
- [67] Duc C., Boukhenane M.-L., Wojkiewicz J.-L., Redon N.: Hydrogen sulfide detection by sensors based on conductive polymers: A review. *Frontiers in Materials*, **7**, 215 (2020).
<https://doi.org/10.3389/fmats.2020.00215>
- [68] Agbor N. E., Petty M. C., Monkman A. P.: Polyaniline thin films for gas sensing. *Sensors and Actuators B: Chemical*, **28**, 173–179 (1995).
[https://doi.org/10.1016/0925-4005\(95\)01725-9](https://doi.org/10.1016/0925-4005(95)01725-9)
- [69] Mousavi S., Kang K., Park J., Park I.: A room temperature hydrogen sulfide gas sensor based on electrospun polyaniline-polyethylene oxide nanofibers directly written on flexible substrates. *RSC Advances*, **6**, 104131–104138 (2016).
<https://doi.org/10.1039/C6RA20710C>